DOI: 10.1002/ ((please add manuscript number))
Full Paper

Ligand-free synthesis of Aluminum-doped Zinc Oxide nanocrystals and their use as optical spacers in color tuned high-efficient organic solar cells

Meriem Gaceur[1], Sadok Ben Dkhil[1], David Duché[2], Fatima Bencheikh[2], Jean-Jacques Simon[2], Ludovic Escoubas[2], Mahdi Mansour[3], Antonio Guerrero[3], Germà Garcia-Belmonte[3], Xianjie Liu[4], Mats Fahlman[4], Walid Dachraoui[1], Abdou Karim Diallo[1], Christine Videlot-Ackermann[1], Olivier Margeat[1]*, Jörg Ackermann[1]*

[1] Dr. M.Gaceur, Dr. S.Ben Dkhil, Dr. W.Dachraoui, Dr. A.K.Diallo, Dr. C.Videlot-Ackermann, Dr. O.Margeat, Dr. J.Ackermann
Aix-Marseille Université, CNRS, CINaM UMR 7325, 13288 Marseille, France
Email: olivier.margeat@univ-amu.fr; ackermann@cinam.univ-mrs.fr

[2] Dr. D.Duché, Ms. F.Bencheikh, Dr. J-J.Simon, Dr. L.Escoubas
Aix Marseille Université, CNRS, Université de Toulon, IM2NP UMR 7334, 13397, Marseille, France

[3] Mr. M.Mansour, Dr. A.Guerrero, Prof. G.Garcia-Belmonte
Institute of Advanced Materials (INAM), Universitat Jaume I, 12071 Castelló, Spain

[4] Dr. X.Liu, Dr. M.Fahlman
Department of Physics, Chemistry and Biology Linkoping University, 58183 Linkoping, Sweden

---

Keywords:
azo, zinc oxide, nanocrystals, interfacial layer, organic solar cell

---

Abstract:

The color of polymer solar cells using an opaque electrode is given by the reflected light, which depends on the composition and thickness of each layer of the device. Metal oxide based optical spacers were intensively studied in polymer solar cells aiming to optimize the light absorption. However, the low conductivity of materials such as ZnO and TiO_2 limits the thickness of such optical spacers to tenth of nanometers. A novel synthesis route of cluster free AZO nanocrystals is presented for solution processing of highly conductive layers without need of temperature annealing, including thick optical spacers on top of polymer blends. The processing of 80 nm thick optical spacers based on AZO nanocrystal solutions on

top of 200 nm thick polymer blend layer is demonstrated leading to improved photocurrent density of 17% compared to solar cells using standard active layers of 90 nm in combination with thin ZnO based optical spacers. These AZO nanocrystals also open new opportunities for the processing of high-efficiency color tuned solar cells. For the first time it is shown that applying solution processed thick optical spacer with polymer blend of different thicknesses can process solar cells of similar efficiency over 7% but of different colors.

---

1. Introduction

Organic solar cells are ones amongst the most relevant approaches for future low cost solar cells thanks to their easy solution processing combined with high efficiency. Intense researches in new polymers or oligomers could increase power conversion efficiency (PCE) beyond the 10% threshold.[1] The optoelectronic properties of the photoactive layer dominate the photocurrent generation and thus the efficiency of the solar cell. The interfacial layers (ILs) sandwiching the photoactive layer are also of high interest due to their different tasks: improve charge carrier extraction towards the electrodes, avoid non-ohmic contact losses as well as avoid charge carrier recombination and exciton quenching at the interfaces.[2] Amongst solution-processed interfacial materials, metal oxides such as Zinc Oxide (ZnO)[3] and Titanium dioxide (TiO_2)[4] are the most studied materials as Electron Extraction Layer (EEL) thanks to their well-adapted energy levels for electron extraction from the fullerene derivatives and their relative ease of elaboration through solution-based nanocrystals syntheses or sol-gel procedures.[3-5] The demonstration of polymer solar cells with high efficiencies beyond 10% and fill factor up to 74% that use solution-processed metal oxide materials as EEL reveal that these materials compete with the best performing interfacial

layers processed by evaporation techniques.[6] Beside their electronic properties, such metal oxide layers introduce so called optical spacer (OSP) effects that modify the light distribution inside the solar cell using regular device structures.[7] Indeed, optical spacers placed between the active layer and the cathode allow improving spatial distribution of light inside the multilayer stack of the solar cell and thus optimizing the absorption in the photoactive layer. Usually metal oxide based optical spacers are very thin layers about 20-30 nm thick due to their low conductivity.[8] However for large-scale solution-processing, the use of thick layers for both photoactive as well as interfacial layers is more adapted for large-scale solution-processing at industrial level. Additionally, to enlarge the benefits of OSP effects in a regular device structure, EEL should be finely adjustable on a wide range of thicknesses in order to precisely tune absorption in the active layer. Brabec and coll. have shown for inverted device structures that conductivity of ZnO EELs can be increased via doping the oxide with Aluminum. This allowed processing of solar cells using thick EELs without losses in device performance.[9] These Al-doped ZnO (AZO) layers were sol-gel processed on ITO and required annealing temperatures of 140-260°C to gain high conductivity, which is compatible only with devices using inverted structures as AZO is deposited onto ITO. However, in regular structures where the metal oxide layer is processed on to organic active layers, such high temperature annealing are prohibited due to strong degradation of these devices under thermal annealing.[10] One possibility to overcome the annealing step applied in sol-gel processes is the colloidal synthesis of highly conductive metal oxide nanocrystals (NCs) such as AZO NCs. In this case, Al doping generates free charges and thus highly conductive properties inside the nanocrystals already during synthesis. There are mainly two synthetic strategies for Al-doped ZnO nanocrystals. AZO nanoparticles can be synthesized via high temperature approache. This approach may yield high-quality monodispersed nanocrystals with controllable size, shape and decent crystalline features, but involves the use of bulky organic ligands for the growth control.[11] Consequently, high post-annealing temperatures over 200°C are needed to

remove the insulating surface ligands in the NCs-based layers in order to generate high conductivity. These high temperatures make their use as interfacial layers in regular device structures difficult due to the strong degradation of polymer solar cells under thermal stress.[12] Colloidal syntheses of other doped metal oxide materials (ITO or IZO[13], ATO[14], AZO[11] and GZO[15]) have also been reported. While the as-synthesized nanoparticles were extremely aggregated resulting in milky suspensions, surfactant-protected GZO colloids resulted in highly soluble NCs solution that could be processed into high quality transparent layers. However, again several strategies to gain high conductivity had to be used, such as UV treatments or annealing at 450°C in forming gas atmosphere were needed to remove the organic surfactants. An alternative strategy relies on the hydrolysis of zinc salts in basic solutions occurring at low temperature in the absence of bulky organic ligands. This approach consists in a modified protocol initially developed for ZnO NCs by Pacholski,[16] in which AZO NCs are produced via the introduction of dopant ions into the initial solutions containing the zinc salts. Raccurt's group studied the synthesis of AZO NCs using zinc acetate dehydrate and aluminium isopropylate (2 at.%) as precursors[17] while potassium hydroxide was used as base. Their results suggest an effective homogeneous incorporation of Al in 7 nm ZnO NCs. But the dispersion of the obtained solids, even in the presence of diethanolamine as additional surfactant, gave rise to a opalescent colloids (with aggregates size about 52 nm confirmed by DLS), producing only rough films after deposition not suitable as interfacial layers. Indeed, we recently demonstrated that performance of ZnO based optical spacers is highly affected by the morphology and surface roughness. Only highly smooth closely packed EELs lead to high-efficiency solar cells with high fill factors up to 68%, while an increase in surface roughness lead to strong losses, mainly in fill factor.[5] Importantly high film quality was only achieved with cluster free ZnO NC solution, which highlights the importance of the aggregate free state of NCs inside the solution used for the EEL processing. The potential of highly conductive optical spacers in combination with thick photoactive layers that aims to improve

performance and robustness of polymer solar cells makes the development of ligand as well as cluster free AZO NCs highly desirable.

Here, we present the synthesis of novel AZO NCs that allow fabricating high efficiency solar cells using thick optical spacers without high temperature annealing. The synthesis and detailed analysis of AZO NCs are reported followed by the fabrication of cluster free NCs solutions in isopropanol by using ethanolamine (EA) as surfactant. In this work, novel AZO NCs are processed into thick highly conductive optical spacers with very low film roughness. These AZO layers require only 80°C as post-annealing treatment and are thus compatible with processing of highly efficient polymer solar cells using normal device structures. Furthermore the solution processing and corresponding optical and electrical properties of the AZO layers were studied in polymer solar cells in normal device structures using polymer blends based on low bandgap polymer Poly({4,8-bis[(2-ethylhexyl)oxy]benzo[1,2-b:4,5-b′]dithiophene-2,6-diyl}{3-fluoro-2-[(2-ethylhexyl) carbonyl]thieno[3,4-b]thiophenediyl}) (PTB7) associated with $PC_{70}BM$ as the acceptor material. In order to demonstrate the potential of novel AZO based optical spacers for robust solar cell processing using thick layers, we also focused on processing of efficient PTB7:$PC_{70}BM$ blend layers with thicknesses up to 210 nm. It has been shown recently, that thick layers of the PTB7 blends, typically over 300 nm, are limited by electron collection that leads to losses in power conversion efficiency.[18] The present work show that PTB7:$PC_{70}BM$ blends up to a thickness of 200 nm can be processed leading to highly efficient solar cells with fill factor over or equal to 60%. Indeed, we show that AZO based optical spacers with thickness up to 100 nm leads to solar cells with conversion efficiency up to 7.6 % when combined with photoactive layer of 200 nm thickness, both enhancing strongly the robustness of device processing. More importantly, we could show for the first time that the novel AZO based optical spacers allow color tuning of organic solar cells over a large range by varying the thicknesses of both

optical spacer and polymer blends, opening new opportunities for the use of optical spacer in OPV.

2. Results and discussion

2.1. Synthesis and characterization of AZO nanocrystals

Aluminum doped ZnO are prepared according to the route introduced by Pacholski[16] and Sirringhaus[19] with some modifications.[20] In a typical experiment, AZO nanocrystals were produced by adding zinc acetate, aluminum isopropylate and distilled water into a flask containing anhydrous ethanol. After heating at 80°C during 30 minutes, potassium hydroxide dispersed in ethanol was added dropwise to the flask followed by heating at 80°C during 16 h. The as synthesized AZO NCs were separated from the solution by centrifugation and dispersed in alcohol-based solvents using ethanolamine (EA). By this method, AZO NCs of Al doping levels ranging from 0% (undoped reference) up to 0.8 at.% were produced by varying the initial ratio of the aluminum isopropylate precursor with respect to zinc acetate, and keeping all the other parameters constant. Importantly, nominal doping levels of 1%, 2% and 5% corresponding to initial precursor ratios of aluminum to zinc atoms, have resulted in lower doping levels inside the NCs with 0.03 at.%, 0.37 at.% and 0.80 at.% of aluminum respectively, as determined after synthesis by ICP-MS (see Table 1 for sample names). Further increase of the nominal doping level did not increase the effective doping level indicating a saturation of Al doping inside the NCs using the described synthesis route. Nevertheless, the range of doping levels obtained here is suitable to increase strongly the conductivity of ZnO by the fact that the maximum of conductivity is produced below 2 at.% aluminum doping level.[21]

The morphological properties of the AZO NCs as a function of Al doping level were studied by high-resolution transmission electron microscopy (HR-TEM). Figure 1 shows typical HR-

TEM images of the $AZO_{0.8}$ NCs indicating a narrow size distribution with an average diameter of 10 nm. The HR-TEM analysis further shows that the AZO NCs are monocrystalline, as confirmed by the FFT pattern (insert Fig.1b) oriented along the [001] zone axis. Corresponding HR-TEM analysis of AZO samples as a function of doping level are presented in Fig.S1. It can be seen that the crystalline nature and the mean diameter remain constant independently of the aluminum doping level (see Table 1). X-Ray Diffraction (XRD) analyses were used to investigate the crystal structure of the AZO NCs in details. Results obtained on AZO NCs powders for the different compositions are shown in Fig. S2. The crystalline structure of all AZO NCs remains similar to the undoped ZnO NCs, i.e. a classical wurtzite structure, which was expected by taking into account the low concentration of Aluminum dopant inside the nanocrystals.[17,22]

In order to process thin films and thus optical spacers, isopropanol solutions containing AZO NCs of different concentrations were prepared. Importantly we used ethanolamine to obtain cluster free solution as demonstrated recently.[5] The aggregate size of the AZO NCs within the solution was determined by Dynamic Light Scaterring (DLS) analysis. From Table 1, it can be seen that the size of the aggregate inside the isopropanol-based solutions (prepared using the EA surfactant) corresponds to the size of single NC as determined by electron microscopy. This proves the high quality of the dispersions and represents an unprecedented result for AZO NCs in terms of solubility without the use of bulky or long surfactants. Importantly, the EA modified AZO solutions were stable over a month without occurrence of any NCs aggregation, as confirmed by regular DLS measurements. Optical characterizations of AZO NCs were performed via recording absorption and emission spectra for all Al compositions in isopropanol (Fig. 2a and 2b). We observed the typical band edge absorption of ZnO at 370 nm for all doping levels, with a very slight shift observed when increasing the aluminum content as found already for other synthesis routes.[23] Importantly, there is a lack of light scattering in the visible on the absorption spectra confirming the high quality of the aggregate-free

solutions. The emission spectra of the undoped ZnO ($AZO_{0.00}$) shows a broad band emission centered at 500 nm addressed to the presence of defect state in the ZnO. By increasing the aluminum doping level, we observe a continuous decrease in the defect emission, which results from the passivation effect of the free charge carriers generated via Al doping. Indeed this passivation of the defect states by introducing the aluminum dopant has already been reported and proves well the presence of the aluminum ions within the lattice structure of ZnO nanocrystals.[24]

2.2. AZO layer properties

The AZO layers were prepared by spin-coating the solutions of AZO NCs dispersed in isopropanol, using EA as surfactant, on glass substrates. Absorption and emission spectra of casted AZO NCs films as a function of Al doping level are shown in Figure S3. The absorption spectra of AZO layers show identical absorption to NCs in solution. Importantly, we do not observe any light scattering effect in the films indicating their high quality. As consequence, AZO layers of a thickness up to 140 nm deposited on glass remains completely invisible. We also studied the emission properties of the thin films as a function of Al doping level as shown in Figure S3. In contrary to the studies in solution, we found an almost complete quenching of the defect emission in AZO layers independently of the Al doping level.

We further studied the energy levels of the AZO NCs as a function of the Al doping level. Figure 2c shows XPS (right panel) and UPS (left panel) data of AZO NCs films as a function of Al concentration, while Table S1 shows the corresponding average work function of the different AZO NCs. In all cases, a value around 4.1 eV could be determined which is the value close to the undoped ZnO NCs. Thus there is no significant impact of Al doping on the work function for the synthesized AZO NCs. Importantly, the work function value of 4.1 eV

fits very well to the LUMO level of fullerenes such as $PC_{70}BM$ making the novel AZO NCs highly suitable for electron extraction layers of polymer blends using fullerenes. The valence band edge, defined as the intersection between the leading edge of the frontier peak and the background of the UPS spectra, is located several eV deeper than the hole transporting levels of typical donor polymers used in organic solar cells (including PTB7) ensuring efficient hole-blocking properties of the layers. The Al(2p) core level spectra show a peak with a binding energy similar to aluminum oxide and there is no signal from metallic aluminum above the noise level of the experiment, suggesting that the aluminum is incorporated into the ZnO only as a dopant without formation of metallic Al clusters.

Taking into account the importance of film quality for efficient charge extraction,[5] the surface roughness of the solution-processed AZO NCs films was studied by AFM. As shown in Figure S4 closely packed layers were observed for all Al doping level with a low surface roughness between 2-3 nm. Importantly, increasing film thickness up to 100 nm results in layers of only 2 nm RMS roughness, suggesting their high potential for processing of highly efficient thick optical spacers.

In order to evaluate the charge transport properties of AZO NCs-based films, we produced solution processed field effect transistors by spin-coating AZO NCs onto Au contact structured SiO_2 substrates followed by a drying process of 30 min at 80°C. In the case of undoped ZnO NCs ($AZO_{0.00}$), low carrier mobilities of $3.2 \cdot 10^{-5}$ cm^2/Vs were observed. It has to be pointed out that higher electron mobilities reported in literature are only achieved by applying an annealing steps of either high temperature up to 400°C or under a reducing atmosphere (such as H_2).[24,25] In this study, only a short annealing step of 80°C is applied. This is necessary for compatible reasons with optical spacer processing on top of the polymer blend (see Part 2.3 Solar cell devices). Under this condition, we observe that $AZO_{0.8}$ NC layers show a clear increase in charge carrier mobility to 1.3×10^{-3} cm^2/Vs and thus conductivity by two orders of magnitude compared to undoped $AZO_{0.00}$ indicating a strong

improvement in the electronic properties via the Aluminum doping of the ZnO NCs (Figure S5).

Electrical characterizations were also carried out by Capacitance-Voltage (*C-V*) measurements using a three-electrode electrochemical set-up with glass/ITO/AZO working electrode, Ag/Ag^+ reference and graphite as counterelectrode. Full impedance spectroscopy was recorded in the dark in the frequency range from 20 mHz to 0.1 MHz and the observed arc was fitted to a *RC* combination and the capacitance was extracted. The tendencies of the curves are similar to previously reported results[26] showing a linear region of the Mott-Schottky plot with a positive slope (Figure 3) indicating that the material is *n*-doped. The slope itself provides information on the doping density of the AZO semiconductor. Similar doping densities are observed for the three different formulations tested in all cases doping densities are high typical for highly conductive semiconductors with values between 1.3-1.8×10^{20} cm^{-3} (see Table 2). However, it is important to note that defect density levels can be overestimated as films are porous with large surface area in contact with the liquid electrolyte and we have used the geometrical area for calculation of the doping levels. We notice that conductivity is exclusively enhanced by increasing mobility with Al doping, as carrier density is observed to be rather constant (see previous *C-V* analysis).

2.3. Solar cell devices using AZO EELs

In order to evaluate the potential of AZO NC layers as optical spacer and EEL in polymer solar cells, we processed solar cells using the regular device structure of ITO/PEDOT:PSS/PTB7:$PC_{70}BM$/ZnO/Al identical to our prior work.[5] We selected $AZO_{0.8}$ NC for the processing of thick optical spacers due to higher conductivity compared to undoped ZnO. In order to achieve the best performing solar cells using a ITO/PEDOT:PSS/PTB7:$PC_{70}BM$/$AZO_{0.8}$/Al stack (see Fig. 5), we investigated first the

photonic absorption inside the active layer as a function of both active layer and $AZO_{0.8}$ layer thicknesses using a transfer matrix method.[5] The polymer blend thickness and $AZO_{0.8}$ layer thickness were varied between 0 to 300 nm and 0 to 90 nm, respectively, while the thicknesses of the other layers have been kept constant (150 nm for the ITO layer, 40 nm for the PEDOT:PSS layer and 120 nm for the Al layer). The optical indices of ITO, PEDOT:PSS, Al and PTB7:$PC_{70}BM$ were taken from literature,[5,27] while optical indices of $AZO_{0.8}$ were determined by Spectroscopic Ellipsometry (see Experimental Part and Figure S6). It is worth to mention that the optical indices of $AZO_{0.8}$ are different to undoped ZnO.[5] This leads to small changes in light absorption inside the solar cells compared to devices using undoped ZnO. Figure 4 shows the total number of photons absorbed inside the active layer as a function of active layer thickness for different $AZO_{0.8}$ thicknesses. Two maxima appear in the absorption curve, which are related to interferential phenomena occurring in thin film stacks.[27,28] The first maximum corresponds to blend thicknesses ranging from 50 to 90 nm with the exact position of each maximum depending on the $AZO_{0.8}$ layer thickness. The second maximum is broader with layer thicknesses ranging from 220 to 300 nm, respectively, making it more suitable for robust processing. Importantly, AZO based EELs lead always to a reduction of light absorption inside the active layer for both maxima compared to solar cells processed without EEL. This finding is identical to solar cells using ZnO as optical spacer,[5] As consequence, optimal performance of solar cells using thin active layers is obtained with the thinnest $AZO_{0.8}$ layer of 20 nm.[5] This corresponds to the device referred as “G” on Fig. 4a.. However in the case of the second maximum, the optical properties of AZO based EEL can bring benefits to the solar cell performance. Taking into account that thick PTB7 based layers are critical for reaching high performance[18], the use of thick EELs allows shifting the maximum in light absorption towards thinner active layers. For instance in the case of a 200 nm thick polymer blends, the use of 80 nm thick $AZO_{0.8}$ layers leads to an increase in light absorption of 17% compared to devices of the first maximum (device referred as “B” in

Figure 4a). The total amount of absorbed photons corresponds to 93% of maximum in absorption usually reached for much thicker polymer blends of 275 nm. Taking into account the limited charge transport properties of PTB7:$PC_{70}BM$ blends[18] the reduction in thickness may be relevant to improve device performance. In order to demonstrate this strategy, we first studied processing of PTB7:$PC_{70}BM$ layers with increased layer thickness. We found that reducing deposition speed down to 1000 rpm with additional increasing concentration to 15 mg/ml for PTB7 and 22.5 mg/ml for $PC_{70}BM$, respectively, at constant ratio leads to blend layers of high optical quality up to 200 nm thickness. Further increase in thickness by reducing speed to 850 rpm generates films of almost identical thickness (210 nm) but with strong optical and thus morphological defects at micro-scale.

In order to evaluate the properties of AZO for electron extraction as well as optical spacer effects following our calculations, we processed devices using polymer blends as well as EEL of different thicknesses. $AZO_{0.8}$ nanocrystals were used as EEL and compared to undoped ZnO. The results are shown in Figure 5 and Figure S7 including Tables that summarize the photovoltaic parameters of the devices. Additionally, we selected three high-efficiency devices that fit with the theoretical cells “G”, “Y” and “B” for detailed optical analysis shown in Figure 5 and Figure 6. First we studied the performance of AZO based EELs in solar cells using 90 nm thick polymer blends that corresponds to device optimized for the first maximum in light absorption. Solar cell processed without EEL shows a low solar cell performance of 5.48 % mainly due to the low FF at 57% related to the lack of the EEL. By comparing EEL based on $AZO_{0.8}$ and ZnO layers (20 nm both), strong increase in device performances is observed for both materials due to reduced charge carrier recombination and extraction barriers at the Al/PTB7:$PC_{70}BM$ interface.[5] The corresponding solar cells show PCEs of 7.1% and 7.43% for $AZO_{0.8}$ and ZnO layers, respectively, with identical V_{oc} and J_{sc}. Here, $AZO_{0.8}$ EEL leads to slightly lower FF at 65.1% compared to 68.4% obtained for ZnO. Taking into account that the work function is similar for both materials, the difference in FF can be

addressed to the larger size of AZO NCs (10 nm) compared to ZnO NCs (5 nm) that may be less suitable for producing thin EELs with homogeneous morphology over large areas. In order to evaluate the performance of thick AZO based EELs, we processed solar cells using thick polymer blends that can push light absorption towards the second maximum in Figure 4.Therefore we processed 80 nm thick $AZO_{0.8}$ layers on top of PTB7:$PC_{70}BM$ blends with thicknesses varying from 130 to 210 nm. The results presented in Figure 7 reveal that the obtained photocurrents fit very well the prediction in absorption as a function of blend thickness. Solar cells using 200 nm thick polymer blends show the highest efficiency of 7.59% with a J_{sc} of 17.1 mA.cm^{-2}, V_{oc} = 0.74 V and a FF = 60%. In contrast, solar cells using 210 nm thick blend layers are clearly less efficient although photocurrent was further improved. This is caused by a much lower FF of 55% compared to cells using active layers of 200 nm with FF = 60%. As thickness is almost identical for both devices, the results indicate that the film quality of the active layer has also an impact on the fill factor of the solar cells. Further studies are needed to better understand this effect and will be addressed in future work. Importantly, solar cells using 130 nm thick active layers (« Y » cell) show still very high FF of 64% although thick optical spacers of 80 nm are used. Thus the evaluation of the electronic properties of thick AZO based optical spacers can be done by comparing these data with solar cells using AZO EELs of 20 nm and 90 nm thick active layers (« G » cell). The fill factors are 64% and 65.1%, respectively, and thus unchanged in both cases. This clearly shows that $AZO_{0.8}$ layers are not limiting charge transport inside the solar cells. However in the case of 80 nm thick $AZO_{0.8}$ EELs applied to 200 nm thick active layers, we observe a loss in fill factor from 65.1% to 60% compared to the “Y” solar cell using 130 nm thick polymer blend layers. This drop in FF can be addressed to the limited charge transport of PTB7 based blends as shown recently.[18]

As next step we compare the performance of thick AZO layers with optical spacers using undoped ZnO. This corresponds to the cell “B”, which compares 200 nm thick polymer blend

layers with 80 nm thick $AZO_{0.8}$ or ZnO EELs. While in the case of $AZO_{0.8}$ a PCE of 7.59% efficiency is obtained as mentioned before, the ZnO based device produces a PCE of 5.92% with a J_{sc} of 16.8 mA.cm^{-2}, V_{oc} = 0.7 V and a FF = 50%. While photocurrent is almost identical for both devices using $AZO_{0.8}$ or ZnO, the loss in efficiency of ZnO based devices is mainly related to a strong drop in FF down to 50%.

The better performance of thick $AZO_{0.8}$ EEL is not only expressed in higher FF, but also in higher V_{oc} and J_{sc} values when compared to ZnO. Concerning the J_{sc} values obtained for solar cells using $AZO_{0.8}$, it was predicted that the use of thick active and EEL layers increase the total light absorption inside the polymer blend. By comparing J_{sc} of cells "G" and "B", one can see that the current density is strongly increased from 14.4 to 17.1 mA.cm^{-2} that corresponds to the increase in light absorption inside the polymer blend of 17% as predicted from calculations. The result demonstrates the high potential of combining both thick active layers and EELs for optimizing photocurrent generation and processing highly efficient polymer solar cells that are compatible with robust processing. In the case of solar cells using 20 nm thick $AZO_{0.8}$ layers, the power conversion efficiencies is much lower of 6.04 % with J_{sc} of 16.33 mA.cm^{-2} and a fill factor of only 50%. The strong drop in FF in the case of 20 nm thin $AZO_{0.8}$ layers processed on top of 200 nm thick active layer, which is also observed for ZnO layers of identical thickness as shown in Figure S8, can not be addressed to transport limitation in either the photoactive layer or the EEL as devices using these layers separately show higher FF. The reason for this drop in fill factor is not yet fully understood but may be related to a need of thicker EELs to cover homogeneously thick active layers. Deeper going studies will address this phenomenon in future work.

2.4. Color tuning using AZO EELs

As the developed AZO NCs allow processing of thick EELs without generating losses in fill factor, we study here the possibility to use such optical spacer for color tuning in highly efficient organic solar cells. Color tuning and perception of organic solar cells have already been described by using different approaches such as color filters[29] or adequate active materials and dyes.[30] In the present study, optical spacers in regular device structures do not only modify the amount of light absorbed inside the active layer (see Figure 4a) but also determine the light reflection of the solar cell. In order to estimate the potential of this technique to generate colored polymer solar cells, we calculated the color coordinates of devices in reflection mode as functions of active layer and the $AZO_{0.8}$ spacer thicknesses at an angle of 8°. For each optical spacer thickness, we calculated color coordinates corresponding to the reflected light for active layer thicknesses ranging between 60 and 200 nm. Figure 6a shows the different colors that can be produced by using a combination of PTB7:$PC_{70}BM$ blend and $AZO_{0.8}$ based optical spacers, with a representation into a color coordinate map based on the CIE xyY (1931) model. The three curves shown in the chromaticity diagram correspond to three $AZO_{0.8}$ thicknesses (0, 20 and 80 nm). Each curve depicts the color evolution of the devices according to the active layer thickness. A white arrow indicating the increase of active layer thickness has been added on the chromaticity diagram. One can first notice that the device colors can be strongly tuned by adjusting the active layer thickness. For the thin AZO layers (0 and 20 nm), the devices are green in the case of thin active layer. They become successively light blue, mallow and orange when the active layer thickness is increased. For the 80 nm thick $AZO_{0.8}$ layers, the devices are light blue for the thin active layer thicknesses and become successively yellow and navy blue when the active layer thickness is increased. We selected three cases of solar cells with high efficiencies of 6.73 %, 7.10% and 7.59% to study the colors in details. Figure 6a shows photograph images of these

three solar cells G, Y and B under different observation angles, while the tabular correlates device efficiency with color coordinates. It can be clearly seen that the color of these solar cells, i.e. the distribution of the reflected wavelengths, varies strongly for the three different solar cells, although their performances are similar. A comparison between the calculated and the measured color coordinates of the three solar cells at an angle of 8° is shown on the chromaticity diagram of the figure 6a (see experimental part for details). Importantly, very good agreements were found between the color coordinates obtained from simulations with the different measured colors of the three G, Y and B solar cells. Thus our results show that a large range of color can be produced with this technique making fine-tuning of the color possible via adjusting the AZO optical spacer and active layer thicknesses, thanks to the control in light absorption amount.

3. Conclusion

Metal oxide based optical spacers were already applied to organic solar cells for a decade, but their low conductivity limited their thickness to tenth of nanometers. Here we presented a novel Aluminum-doped ZnO (AZO) nanocrystals synthesis that allows processing of highly conductive optical spacers onto polymer blends without requiring additional high temperature annealing. We demonstrate that solar cells combining AZO layer of 80 nm with 200 nm thick PTB7:$PC_{70}BM$ blends generate power conversion efficiency of 7.6% thanks to strongly improved photocurrent due to the optical spacer effects and high fill factors. The later was possible due to a reduction of polymer blend thickness down to 200 nm, for which the transport properties of polymer blend PTB7:$PC_{70}BM$ were identified as only limiting factor to even further increase power conversion efficiency. Indeed, the 80 nm thick AZO layer shows very good optical spacer and electron extraction layer properties simultaneously leading to very high fill factors over 64%. This not only improves the compatibility of polymer solar

cells with large-scale robust solution processing but also opens new opportunities for the processing of high efficiency colored solar cells. Future work will focus on combination of $AZO_{0.8}$ based optical spacers of varying thicknesses with low band gap polymers not limited by charge transport properties to fully benefit from optimal light absorption and color tuning in combination with robust thick layer processing of solar cells using regular device structures.

4. Experimental Section

Synthesis of highly soluble AZO nanocrystals: All chemicals were purchased from Sigma-Aldrich and used in an argon filled glovebox without further purification. As no ligand are used for the synthesis, a low-temperature route is maintained in order to avoid nanoparticles agglomeration. Thus the choice of the zinc and aluminum precursors is highly important, as they both have to react by hydrolytic decomposition at this low temperature. Zinc acetate ($Zn(CH_3COO)_2$) and aluminum isopropylate ($Al[(CH_3)_2CHO]_3$) have then been chosen for this ability.[16] In a typical experiment that leads to AZO nanocrystals of 0.80% Al doping level, a solution of 0.442 g of potassium hydroxide KOH (Aldrich, 99.99%) in 23 mL of anhydrous ethanol (Aldrich, 99.8%) was added dropwise under argon into a double neck flask containing a solution of 0.779 g of zinc acetate (Aldrich, 99.99%) and 0.046 g of aluminum isopropylate (Aldrich, 98%) in 42 mL of anhydrous ethanol plus 0.25 mL of distilled water at 80 °C under magnetic stirring. After 16 hours at this temperature, the mixture was centrifuged (7800 rpm, 30 mn) and the supernatant discarded. This exact procedure under inert atmosphere with careful control on the amount of water as well as the slow addition of the base is required to avoid any irreversible nanocrystals agglomeration. To obtain the highly soluble AZO nanocrystals solutions, the solid residue was first redispersed into isopropanol (Aldrich Chemicals, 99.5%) before adding a precise quantity of ethanolamine (Aldrich Chemicals, 99%) to give a formulation of 2µL of ethanolamine for 10mg/mL AZO nanocrystals. Nanocrystals with 10 nm as average diameter were formed and dispersed without noticeable

agglomeration. This solution was used (after dilution when needed) to prepare the spin-coated thin films. AZO nanocrystals of various Al doping level were further produced by simply varying the ratio of aluminum to zinc precursor during synthesis while keeping all the other parameters constant.

Characterization Methods: The AZO NCs were characterized by high-resolution transmission electron microscopy (HR-TEM) (JEOL 3010, acceleration voltage of 300 kV). The samples were prepared by drop-casting a diluted isopropanol solution of AZO NCs onto a carbon-coated copper grid. UV-Vis absorption and fluorescence investigations of the AZO NCs in solution were recorded using a Varian CARY 50 spectrophotometer and a CARY Eclipse spectrometer respectively. Size distribution of the NCs within the solution was determined with Differential light scattering methods (DLS) using a NanoZetaSizer from Malvern. Crystallinity of the AZO NCs was measured by X-ray diffraction (XRD) by using a INEL with a linear detector. Photoemission spectroscopy using UV (UPS, HeI 21.2 eV) and X-ray (XPS, monochromatized AlKα 1486.7 eV) light sources were performed at Linkoping University in Sweden. Atomic force microscopy (AFM) was realized using a Nanoscope III in taping mode to study the quality of AZO NCs layers deposited on top of PTB7:PCBM layers.

Transistor measurements: For thin film transistor fabrication, commercial substrates equipped by interdigitated source and drain electrodes purchased from Fraunhofer (Germany) were used. Source and drain electrodes structured by a lift-off technique are deposited on n-doped silicon wafers covered with thermally grown silicon dioxide (SiO_2). Interdigitated electrodes were formed by 30 nm of gold (Au) and 10 nm of an adhesion layer of indium tin oxide (ITO). Such interdigitated TFT structures formed a final channel width W of 10 mm for a channel length L of 5 μm. The capacitance per unit area of 230 nm thick SiO_2 dielectric layers was 14.6×10^{-9} F.cm^{-2}. Prior the deposition of nanoparticles, the substrates were consecutively

cleaned by ultrasonication with acetone, ethanol and rinsed with deionized water. The SiO_2 substrate was then dried and treated with final UV-ozone plasma for 15 min. Trimethylsilation of the Si/SiO_2 surface was carried out by dipping the silicon wafers to hexamethyldisilazane (HMDS) solution at room temperature in a closed container for one night. The capacitance per unit area of HMDS-treated silicon dioxide dielectric layers was 9×10^{-9} F.cm^{-2}. The solution-processable *n*-type semiconductor inks based on Al-doped ZnO were prepared by transferring the synthesized AZO nanoparticles from alcohol solutions to chloroform ($CHCl_3$) at 30 mg/mL. Spin-coating was performed using a spin-coater machine from SET Company (model TP 6000) where time, speed of the run are fixed to 30 sec., 2000 rpm/min, respectively. After the active layer deposition on top of the source and drain electrodes, the coated substrates were annealed into a preheated hot plate at 80°C for 30 min as a post-treatment. Spin-coating and annealing were performed in a nitrogen-filled glove box as well as all the electrical characterizations.

Current-voltage characteristics were performed with a Hewlett-Packard 4140B pico-amperemeter-DC voltage source. The mobilities μ were extracted from the saturation region of the transfer curves with the equation:

$$I_{ds} = \frac{W}{2L} C_i \mu_{sat} \left(V_g - V_t\right)^2$$

where I_{ds} is the drain-source voltage, C_i is the capacitance per unit area of the gate insulator layer ($C_i = 9\times10^{-9}$ F.cm^{-2}), V_g is the gate voltage, V_t is the threshold voltage, and μ_{sat} is the field-effect mobility.

Capacitance-Voltage measurements: Capacitance-Voltage measurements were performed with Autolab PGSTAT-30 equipped with a frequency analyzer module. A small voltage perturbation (20 mV rms) is applied at frequencies from 10 kHz to 1 Hz. A three-electrode configuration was used composed of a working electrode containing AZO, Pt wire as counter

electrode and a standard Ag/AgCl in 3M KCl as reference electrode. The working electrode was prepared by spin coating of a solution of AZO nanoparticles onto a pre-cleaned Glass/ITO electrode followed by 80°C annealing. A propylene carbonate electrolyte 0.1M $LiClO_4$ was used to avoid AZO decomposition. Capacitance-Voltage curves are extracted by fitting the characteristic arc present in the Nyquist plot to resistance and capacitor connected in parallel.

Solar cell fabrication: The organic-BHJ solar cells were prepared following several steps. First the ITO substrates (15 Ω/sq) were cleaned by deionized water, acetone, ethanol and isopropyl alcohol with ultra-sonication. After exposing the cleaned ITO to a UV/ozone treatment for 15 min to reform the surface, a thin layer of poly(3,4- PEDOT:PSS) (Heraeus, CLEVIOS PVP AI 4083) was spin-coated on the cleaned ITO pre-coated glass substrate at the speed of 4000 rpm for 60s followed by heating on a hot- plate at 140 °C for 20 min to obtain a film thickness of ~ 40 nm.The substrates were then transferred to a nitrogen-filled glove box. The PTB7:PC_{70}BM blend solution was prepared from the weight ratio of 1:1.5 and total conentration of 25 mg/ml or 37.5 mg/ml in CB with 0.3 vol.% of DIO processing additive. After stirring overnight at 55°C, the blends were heated to 70°C for 60 min before spin casting. The BHJ thin films (90 nm) were obtained from spin casting the solution (25 mg/ml) at 1800 rpm for 120 s. By increasing the concentration of the polymer to 15 mg/mL, we obtained blend films with a thickness of 120, 130, 160, 200 and 210 nm corresponding to the spin casting speeds of 2500, 2000, 1500, 1000 and 850 rpm, respectively. The active layers were then transferred into high vacuum for 15h. EEL of AZO (or ZnO) nanocrystals were processed by spin-coating AZO (or ZnO) solutions (at different concentrations in isopropanol in order to obtain different thicknesses) on top of the active layers at 1500 rpm for 60 s followed by annealing for 5 min at 80 °C. All processes were done inside the glove box. The top Al metal electrode (120 nm) was thermally evaporated at $1*10^{-6}$ Torr pressure through a

shadow mask and the device area was 0.27 cm^2. For each device configuration, a total of six cells were measured. The current density–voltage (J –V) characteristics of the devices were measured using a Keithley 238 Source Measure Unit inside the glove. Solar cell performance was measured by using a Newport classe AAA 1.5 Global solar simulator (Oriel Sol3ATM model n° 94043A) with an irradiation intensity of 100 mW/cm^2. The light intensity was determined with a Si reference cell (Newport Company, Oriel n° 94043A) calibrated by National Renewable Energy Laboratory (NREL). Spectral mismatch factor (M) was calculated according to a standard procedure,[31] and M value of 1.02 was obtained for the PTB7:PCBM devices. This value was used to correct the measured I_{sc} values of the solar cells to I_{sc} values corresponding to AM1.5G conditions.

Optical simulations of the solar cells:

Spectroscopic Ellipsometry (SE) has been used to extract the optical indices of AZO thin films. The measurements have been performed for wavelengths ranging between 380 and 1000 nm using a Semilab rotating compensator ellipsometer (RCE)) equipped with a microspot which focuses the beam on a very small area of the sample (a circle with a diameter of 100 µm). The layers were coated on Si substrates as the refractive index difference between the silicon substrate and the organic films is high enough to ensure high reflection coefficients at the organic/Si interface. SEA software (Semilab company) was used to fit the SE measurements of tan(Ψ) and cos(Δ) and extract the optical indices n(λ) and k(λ) of the materials. The dielectric functions $\varepsilon = \varepsilon_1 + i * \varepsilon_2$ of the materials have been fitted with a Tauc-Lorentz model that is adequate for the parameterization of the optical functions of amorphous thin films in the interband region.[32] The optical indices of $AZO_{0.8}$ were measured by spectroscopic ellipsometry and are presented in Figure S6. The optical indices of ITO, PEDOT:PSS Aluminum and PTB7:PC_{70}BM were previously measured by spectroscopic ellipsometry.[5,27] Layer thicknesses were determined with a mechanical profilometer in

combination with AFM cross section measurements. The CIE xyY (1931) model has been employed for the color prediction of the organic solar cells. This model allows calculating the normalized color coordinates (x, y) of solar cells from their reflection spectra by taking into account the human eye sensitivity. Using the optical indices of the materials as input parameters, the reflection spectra of the solar cells have been calculated using a transfer matrix method (TMM).[28] The color coordinate measurements of the solar cells have been deduced from their reflection spectra using the CIE xyY (1931) model. The reflection spectra of the cells have been carried out using a Perkin Elmer spectrophotometer Lambda 950.

Supporting Information
Supporting Information is available from the Wiley Online Library or from the author.

Acknowledgements
This work was supported by the EU project "Sunflower" (FP7-ICT-2011-7- contract num. 287594), the SFUMATO – FUI Project AAP12 and Generalitat Valenciana (project ISIC/2012/008 Institute of Nanotechnologies for Clean Energies). The authors thank Serge Nitsche, Damien Chaudanson and Vasile Heresanu from CINaM for their assistance in the use of the TEM and XRD facilities.

References

[1] a) J.D. Chen, C. Cui, Y.Q. Li, L. Zhou, Q.D. Ou, C. Li, Y. Li, J.X. Tang, *Adv. Mater*. **2015**, *27*, 1035; b) Z. He, B. Xiao, F. Liu, H. Wu, Y. Yang, S. Xiao, C. Wang, T.P. Russell, Y. Cao, *Nature Photonics,* **2015**, *9*, 174; c) J. You, L. Dou, K. Yoshimura, T. Kato, K. Ohya, T. Moriarty, K. Emery, C.C Chen, J. Gao, G. Li, Y. Yang, *Nature Comm*. **2012**, *4*, 1446.

[2] R. Po, C. Carbonera, A. Bernardi, N Camaioni, *Energy Environ. Sci*., **2011**, *4*, 285.

[3] a) Z.Q. Liang, Q.F. Zhang, O. Wiranwetchayan, J.T. Xi, Z. Yang, K. Park, C.D. Li, G.Z. Cao, *Adv. Funct. Mater.* **2012**, *22*, 2194; b) S. Woo, W.H. Kim, H. Kim, Y. Yi, H.K. Lyu, Y. Kim, *Adv. Energy Mater*. **2014**, *4*, 1301692.

[4] J. Xiong, B.C. Yang, C.H. Zhou, J.L. Yang, H.C. Duan, W.L. Huang, X. Zhang, X.D. Xia, L. Zhang, H. Huang, Y.L. Gao, *Organic Electronics*, **2014**, *15*, 835.

[5] S. Ben Dkhil, D. Duche, M. Gaceur, A.K. Thakur, F.B. Aboura, L. Escoubas, J.J. Simon, A. Guerrero, J. Bisquert, G. Garcia-Belmonte, Q.Y. Bao, M. Fahlman, C. Videlot-Ackermann, O. Margeat, J. Ackermann, *Adv. En. Mat.* **2014**, *4*(8), 1400805.

[6] S.H. Liao, H.J. Jhuo, P.N. Yeh, Y.S. Cheng, Y.L. Li, Y.H. Lee, S. Sharma, S.A. Chen, *Scientific Reports*, **2014**, *4*, 6813.

[7] a) J.Y. Kim, S.H. Kim, H.H. Lee, K. Lee, W. Ma, X. Gong, A.J. Heeger, *Adv. Mater*. **2006**, *18*, 572; b) J. Gilot, I. Barbu, M.M. Wienk, R.A.J. Janssen, *Appl. Phys. Lett*. **2007**, *91*, 113520; c) A.K.K. Kyaw, D.H. Wang, D. Wynands, J. Zhang, T.Q. Nguyen, G.C. Bazan, A.J. Heeger, *Nano Lett*. **2013**, *13*, 3796.

[8] T. Stubhan, H. Oh, L. Pinna, J. Krantz, I. Litzov, C.J. Brabec, *Organic Electronics,* **2011**, *12*, 1539.

[9] T. Stubhan, I. Litzov, N. Li, M. Salinas, M. Steidl, G. Sauer, K. Forberich, G.J. Matt, M. Halik, C.J. Brabec, *J. Mater. Chem. A*, **2013**, *1*, 6004.

[10] a) Z.M. Beiley, E.T. Hoke, R. Noriega, J. Dacuna, G.F. Burkhard, J.A. Bartelt, A. Salleo, M.F. Toney, M.D. McGehee, *Adv. Energy Mater*. **2011**, *1*, 954; b) C.G. Wu, C.H. Chiang, H.C. Han, *J. Mater. Chem. A*, **2014**, *2*, 5295.

[11] a) T.V. Thu, S. Maenosono, *J. Appl.Phys.* **2010**, *107*, 014308; b) R. Buonsanti, A. Llordes, S. Aloni, B.A. Helms, D.J. Milliron, *Nano Lett*. **2011**, *11*, 4706.

[12] H.C. Wong, Z. Li, C.H. Tan, H. Zhong, Z. Huang, H. Bronstein, I. McCulloch, J.T. Cabral, J.R. Durrant, *ACS Nano*, **2014**, *8*, 1297.

[13] a) J. Puetz, N. Al-Dahoudi, M. Aegerter, *Adv. Eng. Mater*. **2004**, *6*, 733; b) G. Garcia, R. Buonsanti, E.L. Runnerstrom, R.J. Mendelsberg, A. Llordes, A. Anders, T.J. Richardson, D.J. Milliron, *Nano Lett*. **2011**, *11*, 4415; c) J. Lee, S. Lee, G. Li, M.A. Petruska, D.C. Paine, S. Sun, *J. Am. Chem. Soc.* **2012**, *134*, 13410; c) A. Puetz, T. Stubhan, M. Reinhard, O. Loesch, E. Hammarberg, S. Wolf, C. Feldmann, H. Kalt, A. Colsmann, U. Lemmer, *Sol. Energy Mater. Sol. Cells*, **2011,** *95*, 579.

[14] V. Muller, M. Rasp, G. Stefanic, J. Ba, S. Gunther, J. Rathousky, M. Niederberger, D. Fattakhova-Rohlfing, *Chem. Mater*. **2009**, *21*, 5229.

[15] a) E. Della Gaspera, M. Bersani, M. Cittadini, M. Guglielmi, D. Pagani, R. Noriega, S. Mehra, A. Salleo, A. Martucci, *J. Am. Chem. Soc*. **2013**, *135*, 3439; b) H. Wei, M. Li, Z. Ye, Z. Yang, Y. Zhang, *Mater. Lett*. **2011**, *65*, 427.

[16] C. Pacholski, A. Kornowski, H. Weller, *Angew. Chem. Int. Ed.* **2002**, *41*, 1188.

[17] K. Tarasov, O. Raccurt, *J. Nanopart. Res.* **2011**, *13(12)*, 6717.

[18] a) S. Foster, F. Deledalle, A. Mitani, T. Kimura, K-B. Kim, T. Okachi, T. Kirchartz, J. Oguma, K. Miyake, J.R. Durrant, S. Doi, J. Nelson. *Adv. Energy Mat*. **2014**, *4*, 1400311; b) A. Guerrero, N. F. Montcada, J. Ajuria, I. Etxebarria, R. Pacios, G. Garcia-Belmonte, E. Palomares, *J. Mat. Chem. A*, **2013**, *1*, 12345.

[19] B. Sun, H. Sirringhaus, *Nano Lett*. **2005**, *5*, 2408.

[20] A.K. Diallo, M. Gaceur, N. Berton, O. Margeat, J. Ackermann, C. Videlot-Ackermann, *Superlattices and Microstructures*, **2013**, *58*, 144.

[21] a) A. Aprilia, P. Wulandari, V. Suendo, H.R. Hidayat, A. Fujii, M. Ozaki, *Solar Energy Materials & Solar Cells*, **2013**, *111*, 181; b) H.M. Zhou, D.Q. Yi, Z.M. Yu, L.R. Xiao, J. Li, *Thin Solid Films*, **2007**, *515*, 6909.

[22] T.V. Thu, S. Maenosono, *J. App. Phys*., **2010**, *107*, 014308.

[23] P.C. Yao, S.T. Hang, Y.S. Lin, W.T. Yen, Y.C. Lin, *Applied Surf. Sc*., **2010**, *257*, 1441.

[24] J.H. Noh, I.S. Cho, S. Lee, C.M. Cho, H.S. Han, J.S. An, C.H. Kwak, J.Y. Kim, H.S. Jung, J.K. Lee, K.S. Hong, *Phys. Status Solidi A*, **2009**, *206*(9), 2133.

[25] B.S.Ong, C. Li, Y. Li, Y. Wu, R. Loutfy, *J. Am. Chem. Soc*. **2007**, *129*, 2750.

[26] I. Mora-Sero, F. Fabregat-Santiago, B. Denier, J. Bisquert, R. Tena-Zaera, J. Elias, C. Levy-Clement, *App. Phys. Letters*, **2006**, *89*(20), 203117.

[27] D. Duché, E. Drouard, J.J. Simon, L. Escoubas, P.h. Torchio, J. LeRouzo, S. Vedraine, *Sol. Energy Mater. Sol. Cells*, **2011,** *95*, 18.

[28] D. Duché, F. Bencheikh, S. Ben Dkhil, M. Gaceur, N. Berton, O. Margeat, J. Ackermann, J.-J. Simon, L. Escoubas, *Sol. Energy Mater. Sol. Cells*, **2014**, *126*, 197.

[29] H.J. Park, T. Xu, J.Y. Lee, A. Ledbetter, L.J.Guo, *ACS Nano*, **2011**, *5(9)*, 7055.

[30] a) T. Ameri, G. Dennler, C. Waldauf, H. Azimi, A. Seemann, K. Forberich, J. Hauch, M. Scharber, K. Hingerl, C.J. Brabec, *Adv. Funct. Mater*. **2010**, *20*, 1592; b) A. Colsmann, A. Puetz, A. Bauer, J. Hanisch, E. Ahlswede, U. Lemmer, *Adv. Energy Mater*. **2011**, *1*, 599; c) J. Czolk, A. Puetz, D. Kutsarov, M. Reinhard, U. Lemmer, A. Colsmann, A*dv. Energy Mater.* **2013**, *3*, 386.

[31] V. Shrotriya, G. Li, Y. Yao, T. Moriarty, K. Emery, Y. Yang, *Adv. Funct. Mater*. **2006**, *16*, 2016.

[32] a) G.E. Jellison, F.A. Modine, *Appl. Phys. Lett*., **1996**, *69*, 371; b) G.E. Jellison, F.A. Modine, *Appl. Phys. Lett*., **1996**, *69*, 2137.

Sample names	Input Al%	ICP-MS Al at.%	d_{TEM} (nm)	d_{DLS} (nm)
$AZO_{0.00}$	0	0	10.3	13.9
$AZO_{0.03}$	1	0.03	11.0	12.5
$AZO_{0.37}$	2	0.37	10.9	11.8
$AZO_{0.80}$	5	0.80	10.9	10.2

Table 1. Names of AZO NCs samples, Al% input for synthesis, ICP-MS values of Aluminum at.% content in the NCs, and nanocrystal diameter determined by TEM and DLS analyses.

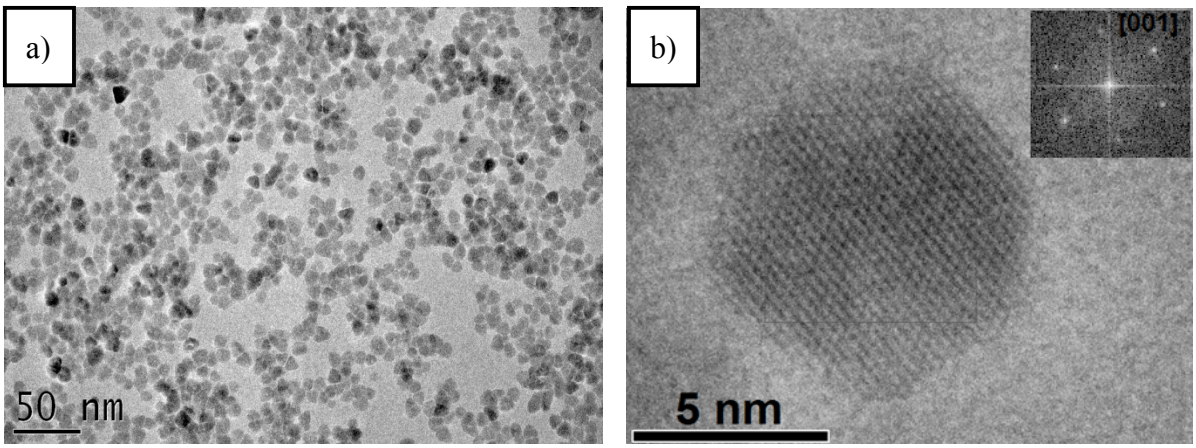

Figure 1. HRTEM images for $AZO_{0.8}$ sample. a) Overall view and b) Single NC (insert: FFT pattern)

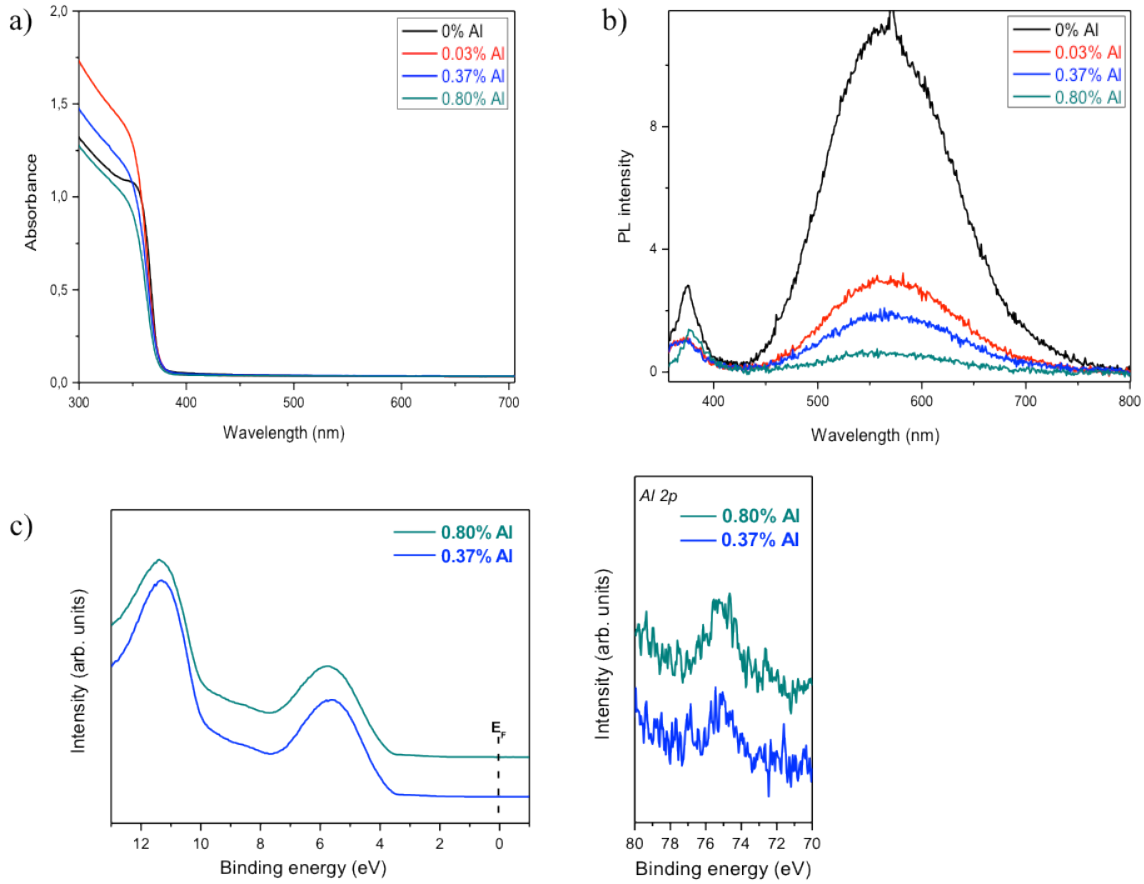

Figure 2. a) UV-vis absorption spectra and b) emission spectra (excitation at 315nm) for all samples. c) XPS/UPS spectra for $AZO_{0.37}$ and $AZO_{0.80}$.

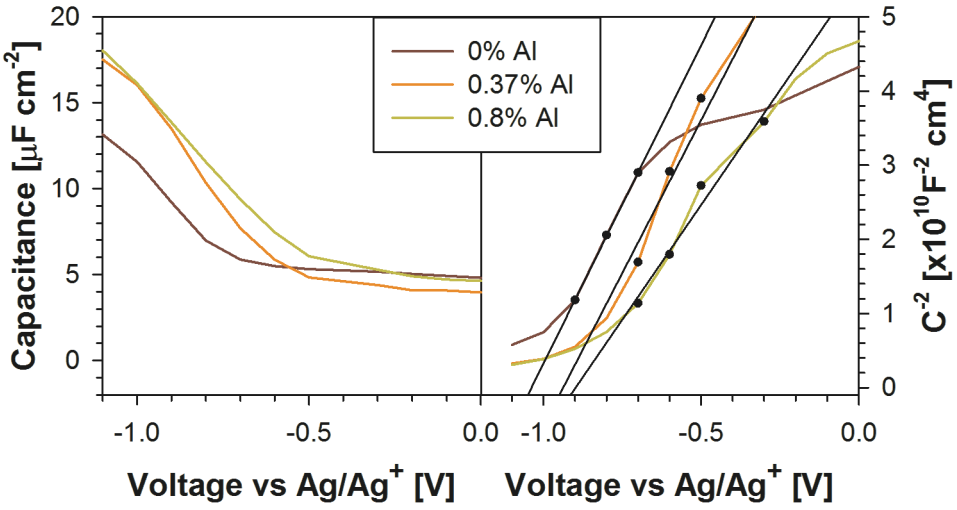

Figure 3. Mott-Schottky analysis for working electrodes in the configuration glass/ITO/AZO with different Al compositions.

Samples	$AZO_{0.00}$	$AZO_{0.37}$	$AZO_{0.80}$
n [10^{20} cm^{-3}]	1.6	1.3	1.8

Table 2. Summary of parameters extracted from Capacitance-Voltage measurements of samples in the configuration glass/ITO/AZO with different Al compositions.

a)

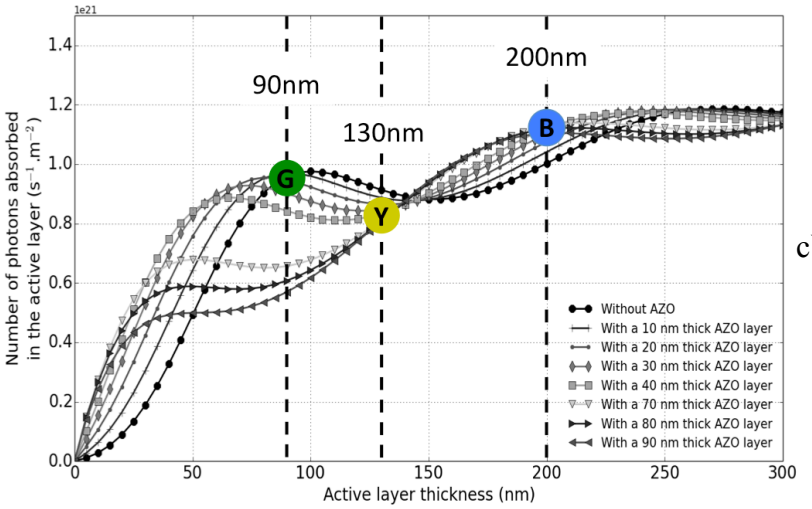

b)

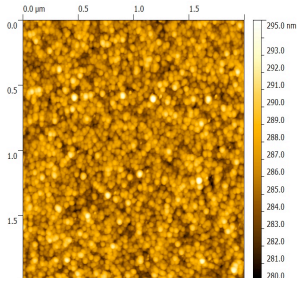

c)

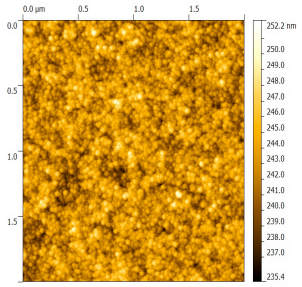

Figure 4. a) Theoretical absorption in the active layer as a function of active layer thickness (B,Y and G refers to the studied solar cells).
AFM for $AZO_{0.8}$ layers with different thickness: b) 20nm (RMS=1.77nm) and c) 80nm (RMS=1.98nm).

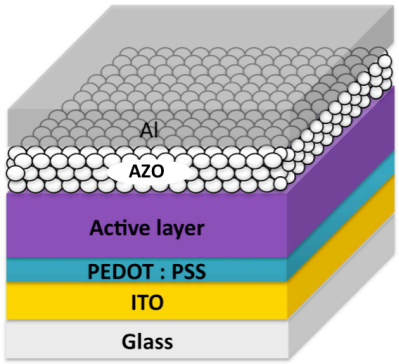

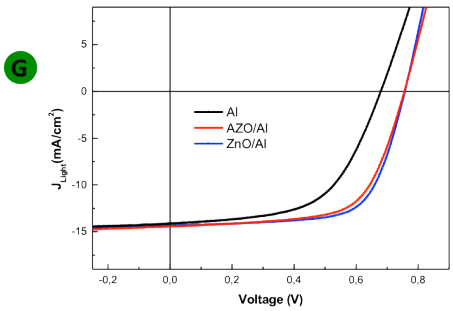

ITO/PEDOT:PSS/PTB7-PCBM/EEL/Al

90 nm PTB7/PCBM	PCE (%)	V_{oc} (mV)	J_{sc} (mA.cm^{-2})	FF (%)	Average PCE (± std. dev.) (%)
No EEL	5.48	0.68	14.1	57.0	5.24 ± 0.20
AZO - 20 nm	7.10	0.76	14.4	65.1	6.99 ± 0.09
ZnO - 20 nm	7.43	0.76	14.3	68.4	7.38 ± 0.06

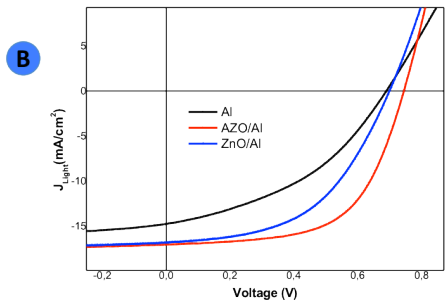

ITO/PEDOT:PSS/PTB7-PCBM/EEL/Al

200 nm PTB7/PCBM	PCE (%)	V_{oc} (mV)	J_{sc} (mA.cm^{-2})	FF (%)	Average PCE (± std. dev.) (%)
No EEL	4.17	0.69	14.8	41	3.94 ± 0.15
AZO - 80 nm	7.59	0.74	17.1	60	7.56 ± 0.03
ZnO - 80 nm	5.92	0.70	16.8	50	5.86 ± 0.05

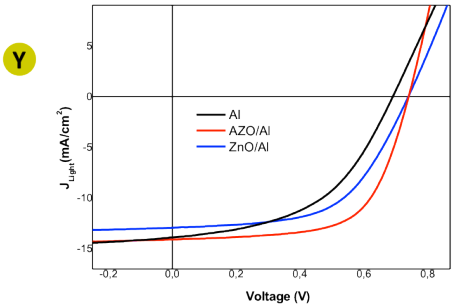

ITO/PEDOT:PSS/PTB7-PCBM/EEL/Al

130 nm PTB7/PCBM	PCE (%)	V_{oc} (mV)	J_{sc} (mA.cm^{-2})	FF (%)	Average PCE (± std. dev.) (%)
No EEL	4.70	0.69	13.9	49	4.36 ± 0.29
AZO - 80 nm	6.73	0.74	14.1	64	6.67 ± 0.05
ZnO - 80 nm	5.40	0.73	12.9	56.4	5.34 ± 0.04

Figure 5. J(V) curves under illumination for the three G, B and Y cells using bare aluminum contact, $AZO_{0.8}$ and ZnO as interfacial layers.

a)

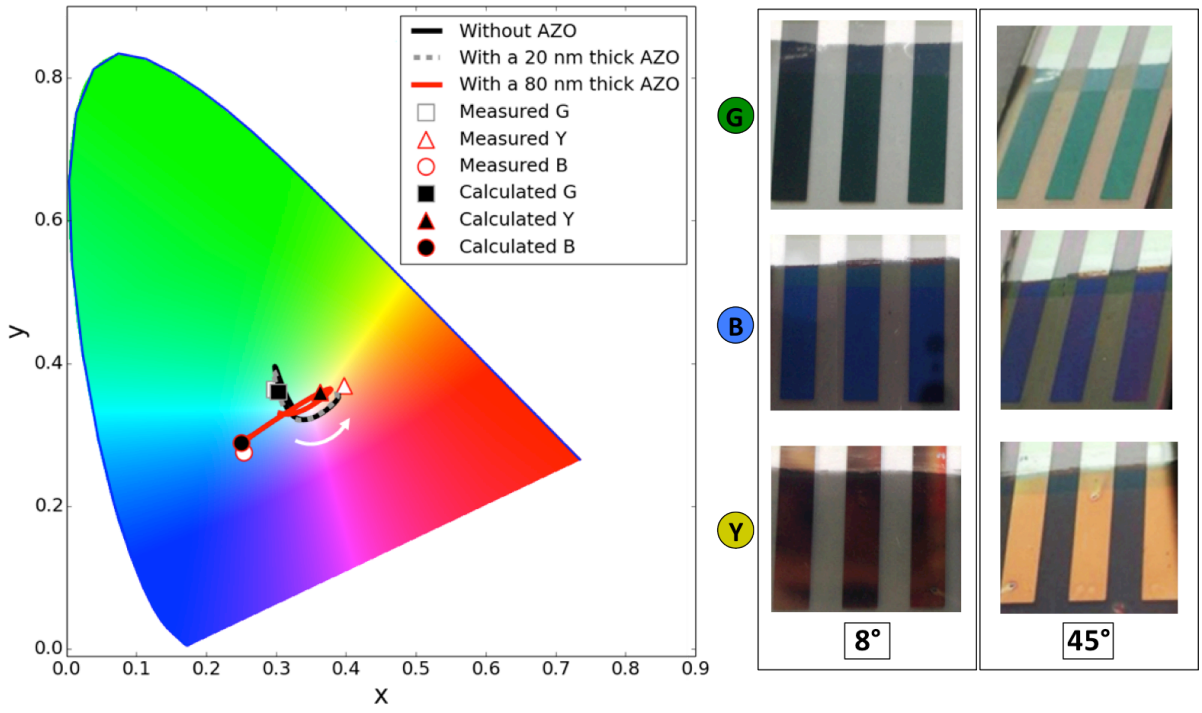

b)

Cells names	PCE	Active layer thickness	$AZO_{0.8}$ layer thickness	Measured color coordinates	Calculated color coordinates
G	7.10 %	90 nm	20 nm	(0.30, 0.36)	(0.30, 0.36)
B	7.59 %	200 nm	80 nm	(0.25, 0.28)	(0.25, 0.29)
Y	6.73 %	130 nm	80 nm	(0.4, 0.37)	(0.36, 0.36)

Figure 6. a) Predicted color as a function of active layer and $AZO_{0.8}$ thicknesses (left) and photograph images of the Green, Blue and Yellow solar cells at 8° and 45° (right).
b) Measured and calculated color coordinates (at 8°) for the different cells.